

Effect of high anodic polarization on the passive layer properties of superduplex stainless steel friction stir welds at different chloride electrolyte pH values and temperatures

L.A. Santa-Cruz^{1,2)}, G. Machado²⁾, A.A. Vicente³⁾, T.F.C. Hermenegildo¹⁾, and T.F.A. Santos¹⁾

1) Department of Mechanical Engineering, Universidade Federal de Pernambuco, Av. da Arquitetura, s/n, 50740-550, Recife, PE, Brazil

2) Center of Nanotechnology, Centro de Tecnologias Estratégicas do Nordeste, CETENE, Recife, PE, Brazil

3) Department of Chemical Engineering, Universidade de São Paulo, São Paulo, SP, Brazil

(Received: 26 August 2018; revised: 27 November 2018; accepted: 1 January 2019)

Abstract: The conditions used for friction stir welding of duplex stainless steels determine the resulting mechanical and corrosion performance of the material. This study investigates the corrosion resistance of UNS S32750 and S32760 superduplex stainless steels (SDSSs) joined by friction stir welding, employing cyclic polarization, Mott–Schottky, and microscopy techniques for analysis. The microscopy images indicated the presence of a deleterious intermetallic phase after electrolytic etching of S32760, as well as decreased corrosion resistance. The presence of molybdenum in the steels promoted better passive behavior at low pH. The Mott–Schottky curves revealed p-n heterojunction behavior of the passive oxide. Images acquired after the polarization test by scanning electron microscopy showed higher passivation propensity with increases of temperature and pH.

Keywords: superduplex stainless steel; friction stir welding; corrosion resistance; cyclic polarization; Mott–Schottky

1. Introduction

Superduplex stainless steels (SDSS) show a biphasic ferrite and austenite structure, which combines corrosion resistance with excellent mechanical properties [1]. However, the precipitation of undesired phases during welding processes or hot operations can lead to loss of corrosion resistance [2]. Fusion welding of SDSS can lead to disruption of the equilibrium of the ferrite and austenite phases, with precipitation of intermetallic phases. However, the use of the friction stir welding (FSW) can reduce some of the problems caused by fusion of the material as it enables the joining of materials below their fusion temperatures [3].

Many studies have shown the influence of the welding process on the emergence of deleterious phases that affect the corrosion resistance of stainless steels [4–8]. However, few reports have related the presence of deleterious phase to the properties of the passive film that was formed, or have performed extended corrosion evaluations. Most investiga-

tions concerning passive layer properties have focused on the base metal [9–11].

Different environment variables can cause changes in the passive film, such as the presence of halides in solutions, pH and temperature, because they affect the kinetics of the electrochemical reactions [12–14]. High acidity of the medium is known to increase the corrosion rate [15–16]. As a result, additions of alloying elements are used to reduce pitting by improving the passive behavior of the material [17]. In the investigation of the dependence of electrochemical reactions on temperature, Cui *et al.* [11] showed the influence of temperature on the passivation process of stainless steels, which is considered to be thermally activated. Several studies have reported the effect of temperature on passivity and the corrosion process [11,13,15,18–19]. A higher temperature exerts two different effects in the corrosion process as it increases the kinetics of the anodic and cathodic reactions.

Additionally, in some cases, high anodic polarization after the oxygen evolution potential can also affect the passive

Corresponding author: T.F.A. Santos E-mail: tiago.felipe@ufpe.br

© University of Science and Technology Beijing and Springer-Verlag GmbH Germany, part of Springer Nature 2019

layer properties, depending on the type of semiconductor [20]. A good electron conductor allows water oxidation, since electrons can be withdrawn from the water molecules and travel through the oxide to the metal. Hence, when oxygen evolution occurs on the anode, the polarization curves show an increase in the density current with higher potential [21].

Given the high corrosion resistance of SDSSs, the aim of this work was to distinguish between the passivation behaviors of friction stir welds produced using two SDSSs with similar compositions, under extremely aggressive high anodic polarization by employing cyclic polarization curves. In addition, different conditions of pH and temperature were used to elucidate their effects in the passivation and corrosion processes. Mott–Schottky analysis was used to determine the oxide conductivity and to establish whether oxygen evolution occurred at the anode. UNS S32750 and S32760

SDSSs were submitted for FSW. The samples were characterized by optical microscopy prior to obtaining the polarization curves. After the measurements, the materials were analyzed by scanning electron microscopy (SEM). Previous works highlighted aspects of the processes used for welding these steels using FSW technology, as well as the thermal cycle of the steel during welding [22–23], the use of a ceramic backing plate during welding [24], and analysis of the response parameters for welding of the steels considered in this work with extensive microstructural characterization [25–26].

2. Experimental

The base metal chemical compositions, shown in Table 1, were provided by Outokumpu (for UNS S32750) and Weir Materials (for UNS S32760).

Table 1. Chemical compositions of the steel alloys

wt%

UNS	C	Si	Mn	Cr	Ni	Mo	W	Cu	N	P	S
S32750	0.02	0.25	0.78	24.9	6.88	3.79	—	0.34	0.26	0.023	0.001
S32760	0.02	0.35	0.64	25.2	7.00	3.70	0.62	0.62	0.23	0.024	0.002

Steel plates measuring 500 mm × 180 mm × 6.0 mm were used for preparation of the FSW joint samples. The joints were formed using a dedicated FSW system (Transformation Technologies, Inc.) that allowed position and force control during welding. A downforce of 37 kN was necessary to produce sound welds using an untilted composite of polycrystalline cubic boron nitride in a metallic matrix of 40vol%W–Re (PCBN–40%W–Re). The tool had a shoulder diameter of 25 mm and a length of 6.0 mm. Welding speeds were limited to keep the forces in the welding direction at or below 10 kN and to extend the life of the tool. The final operating parameters for SDSS were 200 r/min and 100 mm/min. Details concerning the welding process, parameters evolution, and other aspects of the welding procedure are provided in previous works [25–26].

Cyclic polarization tests in 3.5wt% NaCl solution were performed with the FSW joints and the base metal using a Metrohm Autolab 128N potentiostat galvanostat in a three-electrode electrochemical cell fitted with an Ag/AgCl (3 M KCl) reference electrode (RE), a platinum counter electrode (CE), and the working electrode (WE). The tests were applied at the top of the weld (the weld bead area used was approximately 17 mm × 20 mm), where the area exposed to the electrolyte was 1 cm² (diameter of approximately 11.3 mm), such that only the stir zone was considered, as shown in Fig. 1. It is important to highlight that there was non-uniformity of the joint in the transverse section, while at the top of the weld bead, non-uniformity was

observed at the stir zone/base metal interfaces. Hence, problems of microstructural non-uniformity in the welded joint were not considered in this work. Measurements were obtained at 25°C and pH 5.9 for all samples, while 65°C and pH 3.0 were only employed for the welded joint. The scanning speed was 0.001 V/s, with a reversal current of 1 mA and initial potential of –0.7 V vs. Ag/AgCl below the open circuit potential (E_{OC}), at which the corrosion potential test ended (2.2 V vs. Ag/AgCl) after the oxygen equilibrium potential to identify the electrochemical behavior.

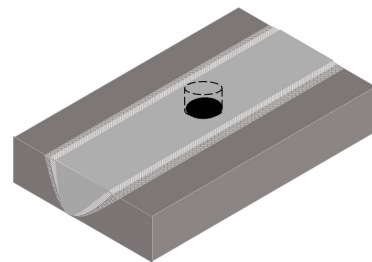


Fig. 1. Region of the stir zone of the welded joint exposed to the electrolyte.

The metallographic preparation of the samples consisted of abrasion using water-resistant sandpaper with granulometry from 180 to 1500 mesh, followed by polishing using diamond with granulometry of 3 and 1 μm. To reveal the presence of any deleterious phases, a solution of 40wt% NaOH in distilled water was used to visualize the microstructure using etching, as described in ASTM A923 (2008). In some cases, 60vol% HNO₃ was used. Microstructural

characterization was performed using an Olympus GX51M optical microscope and Quanta FEG 650 and Hitachi TM3000 scanning electron microscopes.

For Mott–Schottky analysis, the samples were polished and stored in air for several weeks for natural formation of the passive film. Subsequently, electrochemical measurements were performed in a solution of 0.5 M sodium sulfite (Na_2SO_3) with the addition of 0.1 M sodium chloride in distilled water (solution pH 9.61). Mott–Schottky plots were obtained using a frequency of 1000 Hz at 0.01 V amplitude, for a range of applied potentials, with a step potential of 0.27 V. The potential measured vs. Ag/AgCl ($E_{\text{Ag/AgCl}}$) can be converted to the reversible hydrogen electrode (RHE) scale (E_{RHE}) according to the following relation:

$$E_{\text{RHE}} = E_{\text{Ag/AgCl}} + 0.059 \times \text{pH} + 0.197 \quad (1)$$

3. Results and discussion

3.1. Microstructural characteristics of the SDSS FSW joints

For the detection of deleterious intermetallic phases in duplex stainless steels, electrolytic etching was performed as recommended in ASTM A923 with 40wt% NaOH in distilled water. The methodology described in ASTM A923 [27] was used to identify the presence of intermetallic phases in the welded joints, especially the sigma phase. Procedure A of the standard method enables fast identification of samples that are free of deleterious intermetallic phases. Although this procedure could not precisely identify the nature of the intermetallic phases, it could provide evidence of their effects.

Fig. 2 shows the various regions typically observed in the joining of steels by FSW, in this case for SDSS UNS

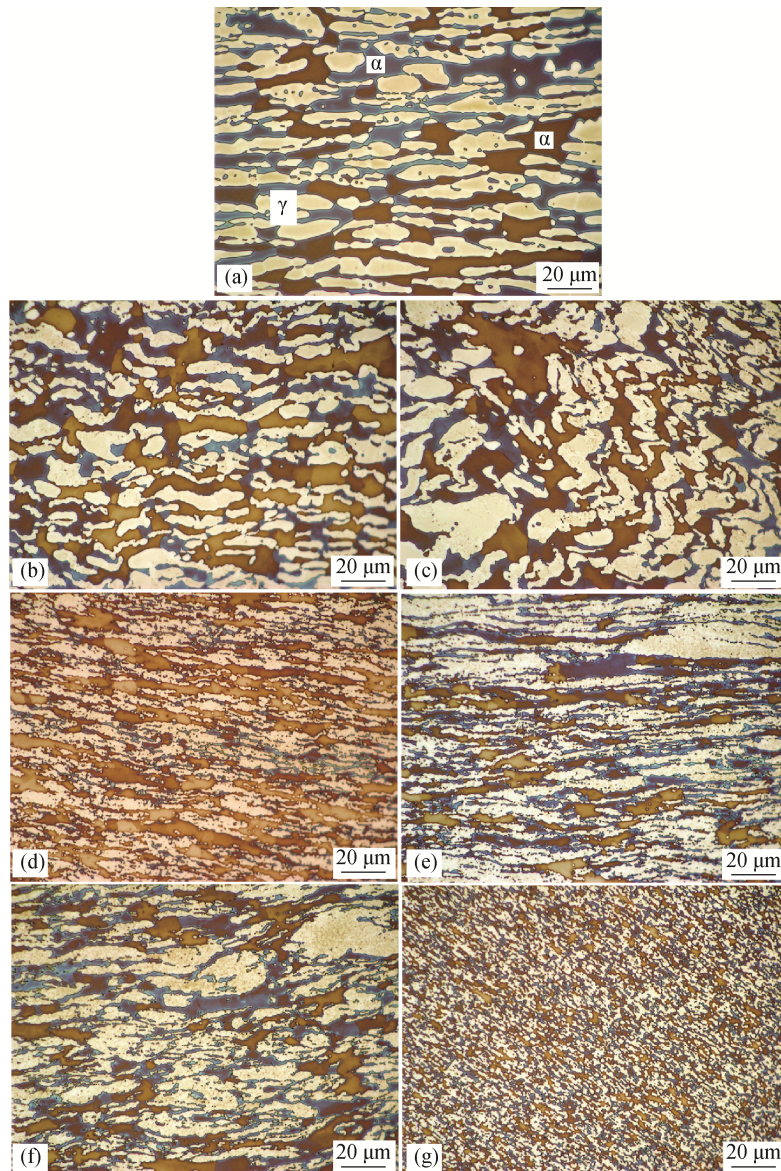


Fig. 2. Regions of the welded joint of SDSS UNS S32750: (a) BM; (b) TMAZ-RS; (c) TMAZ-AS; (d) SZ-root; (e) SZ; (f) SZ-RS; (g) SZ-AS. Electrolytic etching: 40wt% NaOH in distilled water.

S32750. The micrograph shows the base metal (BM), stir zone (SZ), stir zone retreating side (SZ-RS), stir zone advancing side (SZ-AS), root of the FSW joint (SZ-root), thermomechanically affected zone retreating side (TMAZ-RS), and thermomechanically affected zone advancing side (TMAZ-AS). According to Mishra *et al.* [4], these regions arise due to geometric characteristics of the tool and the complex movement of the material, causing gradients of deformation, temperature, and deformation rate. Fig. 2(a) shows the typical laminar structure of austenite (γ) and ferrite (α) of the BM. The TMAZ-RS and TMAZ-AS regions are shown in Figs. 2(b) and 2(c), respectively. The deformed lamellae of austenite (white color) was observed within a ferritic matrix (tones varying from brown to blue).

The NaOH solution preferentially attacked the ferrite,

with this phase presenting a range of tones from brown to blue, indicative of differences in its susceptibility to chemical resistance. However, the austenite showed no color change during chemical attack, demonstrating that it did not react electrochemically. In the SZ regions of the S32750 FSW joints, shown in Figs. 2(d)–2(f), islands of austenite were discerned in the ferritic matrix as has been observed using optical microscopy [28]. The SZ-AS, as shown in Fig. 2(g), presented a clearly refined structure, with equiaxial grains evidence of the recrystallization process. However, none of the micrographs revealed pitting or corroded areas, which should have occurred if the structure were affected by the attack, according to the ASTM standard.

Fig. 3 shows the different regions of a welded joint of the UNS S32760 steel. The same characteristic microstructures

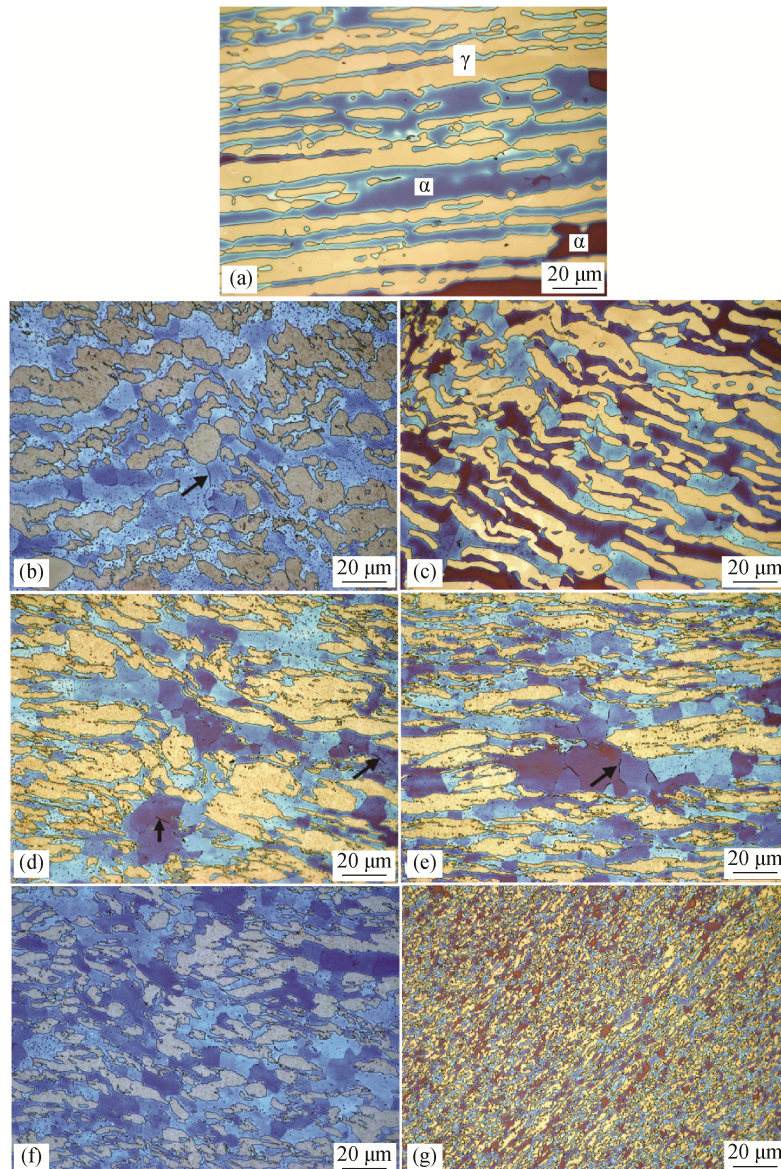


Fig. 3. Regions of the welded joint of SDSS UNS S32760: (a) BM; (b) TMAZ-RS; (c) TMAZ-AS; (d) SZ-root; (e) SZ; (f) SZ-RS; (g) SZ-AS. Electrolytic etching: 40wt% NaOH in distilled water.

were observed as previously described. However, localized attack at the boundaries of the ferrite–ferrite grains was indicative of the possible presence of a deleterious intermetallic phase. The arrows in Fig. 3 indicate the affected areas, located mainly in the SZ and SZ-root regions. The high number of microalloying elements present in these steels means that the risk of precipitation of intermetallic phases limits the thermal input and interpass temperature during fusion welding [29]. In the case of FSW, the thermal cycle subjects the material to high temperatures in a shorter period of time (due to higher heating rates) [18], which may be sufficient to promote the precipitation of deleterious phases.

3.2. Cyclic polarization and effects of pH value and temperature

Polarization tests at different pH values and temperatures were performed with the SDSSs. According to the results in Section 3.1, presence of a deleterious phase in the S32760 was observed based on the ASTM A923 standard procedure. As a result, the potential applied for the polarization curves was swept to 2.2 V vs. Ag/AgCl, after the oxygen equilibrium potential, to identify the differences in electrochemi-

cal behavior between the UNS S32750 and S32760. The high polarization forced the materials to remain in the transpassive state for a long time. Hence, the effects reported in this section are not representative of real corrosion, but provide an understanding of how the presence of a deleterious phase can influence the formation of the oxide layer.

Cyclic polarization curves were obtained for the stir zones of S32750 and S32760 in the 3.5wt% NaCl solution. Fig. 4 shows the cyclic polarization curves as a relation between pH value and temperature. 25°C with pH 5.9 was applied for all of the samples and 65°C with pH 3.0 was applied for only the welded joints. For the potential scanning range employed, the graphs showed well-defined passive and transpassive regions. The transpassive region starts at the breakdown potential (E_b), with the current density increasing as the potential increases. All of the graphs presented positive hysteresis, indicating that the samples were not able to fully repassivate after disruption of the passive film [30]. The graphs (Fig. 4) showed no pitting potentials following abrupt increases in corrosion current density and small variations in the potential.

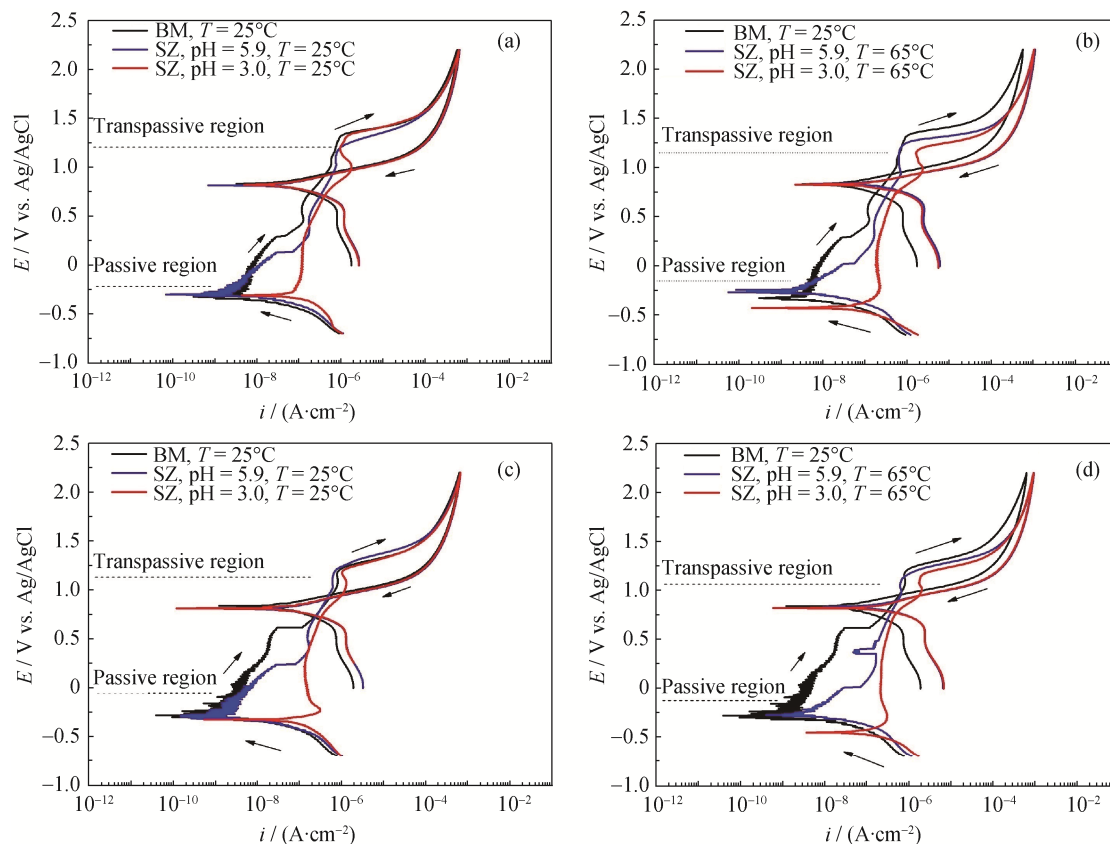


Fig. 4. Cyclic polarization curves obtained in 3.5wt% NaCl electrolyte for the BM (pH 5.9, $T = 25^\circ\text{C}$) and the FSW joint (at pH 5.9, $T = 25^\circ\text{C}$ and pH 3.0) of SDSS UNS S32750 at (a) 25°C and (b) 65°C , and for the S32760 FSW joint at (c) 25°C and (d) 65°C .

Tables 2 and 3 show the data for the corrosion potential (E_{corr}), repassivation potential (E_{rp}), corrosion current density (i_{corr}), breakdown potential (E_{b}), and passive region (ΔE), corresponding to the difference between E_{rp} and E_{corr} . Anodic and cathodic Tafel fittings were performed to calculate E_{corr} and i_{corr} . Initially (with Tafel's own symbols), the Tafel slope related the overpotential (ε) to the current density (J), with parameters a and b being constants [31]:

$$\varepsilon = a + b \times \lg J \quad (2)$$

The SDSS UNS S32760 showed lower E_{b} , E_{rp} , and E_{corr} than S32750. Due to the lower E_{b} and E_{rp} , the transpassive region was reached faster for this material and its repassivation was more difficult. Its corrosion current density values were slightly greater than those for S32750, except when the material was exposed to the electrolyte at 65°C. The better resistance of S32750 was due to the absence of a deleterious phase, as shown in Section 3.1.

Table 2. Corrosion potential, corrosion current density, repassivation potential, breakdown potential, and passive region for the SZ of SDSS UNS S32750 in 3.5wt% NaCl electrolyte, at different pH values and temperatures

pH value	Temperature / °C	$E_{\text{corr}} / \text{V vs. Ag/AgCl}$	$i_{\text{corr}} / (10^{-9} \text{ A}\cdot\text{cm}^{-2})$	$E_{\text{rp}} / \text{V vs. Ag/AgCl}$	$E_{\text{b}} / \text{V vs. Ag/AgCl}$	$\Delta E / \text{V vs. Ag/AgCl}$
5.9	25	-0.24 ± 0.02	2.2 ± 0.4	0.83 ± 0.01	1.30 ± 0.07	1.07
3.0	25	-0.29 ± 0.04	40.4 ± 30.0	0.83 ± 0.02	1.27 ± 0.11	1.12
5.9	65	-0.25 ± 0.01	3.8 ± 0.7	0.84 ± 0.01	1.17 ± 0.07	1.08
3.0	65	-0.37 ± 0.02	68.0 ± 9.0	0.84 ± 0.01	1.20 ± 0.03	1.21

Table 3. Corrosion potential, corrosion current density, repassivation potential, breakdown potential, and passive region for the SZ of SDSS UNS S32760 in 3.5wt% NaCl electrolyte, at different pH values and temperatures

pH value	Temperature / °C	$E_{\text{corr}} / \text{V vs. Ag/AgCl}$	$i_{\text{corr}} / (10^{-9} \text{ A}\cdot\text{cm}^{-2})$	$E_{\text{rp}} / \text{V vs. Ag/AgCl}$	$E_{\text{b}} / \text{V vs. Ag/AgCl}$	$\Delta E / \text{V vs. Ag/AgCl}$
5.9	25	-0.26 ± 0.02	2.5 ± 0.4	0.81 ± 0.02	1.26 ± 0.09	1.07
3.0	25	-0.33 ± 0.03	50.0 ± 20.0	0.81 ± 0.02	1.22 ± 0.01	1.14
5.9	65	-0.26 ± 0.01	3.8 ± 0.7	0.82 ± 0.01	1.15 ± 0.05	1.07
3.0	65	-0.38 ± 0.08	47.8 ± 9.0	0.82 ± 0.02	1.13 ± 0.06	1.19

3.2.1. Influence of pH value on the passive behavior

For the S32750 and S32760 SDSSs, within the passive regions of the graphs, the curves (Fig. 4) for the BM and SZ at pH 5.9 showed instability of the passive film, which was characterized by an increase of the current density with higher applied potential. However, the curves (Fig. 4) obtained at pH 3.0 showed greater inflection for the passive region, indicating that the steels presented better passive behavior in an acid solution. This was also observed with the ΔE data (Tables 2 and 3), with higher values obtained for the acid environment. This improved passive behavior was due to the greater stability of the passive oxides.

The main oxide-forming elements in SDSSs are Cr, Mo, and W (when tungsten is present) [30]. Therefore, evaluation of the thermodynamic stability of the compounds formed by these elements, at room temperature and different pH values, was previously investigated by Pourbaix diagrams at 25°C, using the FACT/FACTSAGE database (2005 update) [32], as shown schematically in Fig. 5. From the Cr, Mo, and W diagrams for pH 3.0 and 5.9, oxide instability was identified at different potentials, since these

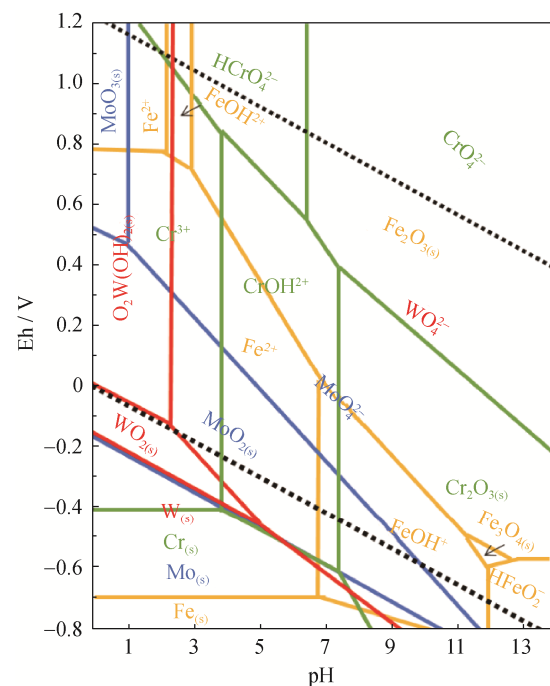


Fig. 5. Thermodynamic stability diagram for the compounds formed by Cr, Mo, and W in SDSSs adapted from Ref. [32].

elements were in the transpassive state. At pH 5.9, the transpassive state started near Eh value of -0.10 V, while at pH 3.0, the region started at a potential near 0.20 V. For these SDSSs, the increase in acidity led to enhanced thermodynamic stability of the passive state for nobler potentials, which could be attributed to the likelihood of the Mo being present under the $\text{MoO}_{2(s)}$ oxide. This result was corroborated the analyses of the effect of Mo in the corrosion process, where it enhanced the passive behavior of stainless steels [17].

For the stainless steels in the presence of chloride, the polarization curves exhibited noise in the passive region, which could be attributed to the nucleation and propagation of unstable pits [12,32]. These pits first grow for a short period and then become inactive due to the passivation process. They do not cause significant damage to the metal. Hence, the results also showed that increased acidity led to greater stability of the oxides in the passive film, despite increasing the nucleation of the metastable pits.

3.2.2. Influence of pH value on the anodic process

An increase in acidity caused substantial increases of nearly 20-fold in the corrosion current densities (i_{corr}) for the samples exposed to the electrolyte at both temperatures. The higher acidity of the electrolyte decreased the work required to initiate the anodic reactions in the material, so the corrosion potentials (E_{corr}) had lower values.

Better passive behavior was observed at a low pH value, but the i_{corr} and E_{corr} values were indicative of increases in the corrosion reactions for both samples. In this work, the acidity of the medium was induced by small additions of HCl to the solution. Therefore, the higher concentration of Cl^- in the solution could have been responsible for the high anodic dissolution. Since the presence of Mo enhanced the passive behavior, it is evident that there is a need for further studies regarding the effect of acidity, without the addition of Cl^- . The passive film can be disrupted by chlorides according to complex mechanisms that can damage the film due to the chemical breakdown of the passivity at high potential [33]. These anions are capable of interacting with stainless steel, consequently increasing dissolution. The generation of an intense anodic dissolution current occurs as a result of the electrochemical reactions that generate electrons.

It is important to consider the difference between the passive behavior and corrosion potential (E_{corr}). The passive behavior is related to the stability of the oxide as the passive region is under a potential at which the oxides are stable. The E_{corr} value indicates the ease with which the anodic reactions can occur, while i_{corr} reflects the quantity of anodic

reactions. In the presence of more chloride, the work required to initiate the anodic reaction is lower, so the quantity of reactions increases.

3.2.3. Double effect of temperature

A higher electrolyte temperature decreased the work required to initiate the anodic reactions, as indicated by the lower E_{corr} , and increased the kinetics of the reactions, as shown by the increase in i_{corr} . Although the variation of E_{tp} was within the error range, the data shown in Tables 2 and 3 suggest that the repassivation of the materials was facilitated, in agreement with previous works [11,14]. The transpassive region was initiated more rapidly at higher temperature.

According to Escrivà-Cerdán *et al.* [19], heating of the solution accelerates the anodic reactions and, consequently, also increases the passive film dissolution rate, especially in the case of solutions containing aggressive halide ions because these ions should facilitate oxide dissolution. The high temperature increases the mobility of chloride ions [11,13], hence enhancing mass transport due to convection, resulting in more porous film in a chloride medium [14,19]. Therefore, the beginning of the transpassive region, determined by E_b , decreases as the temperature increases because the passive film formed is more defective and sensitive to disruption, while the anodic reactions are accelerated.

Cui *et al.* [11] showed that passivation is a thermally-activated process that follows the Arrhenius relationship for SDSS UNS S32750. Throughout the passive range, the mechanism of passivation is the same. Furthermore, in a study of the formation of oxide film on Fe–Cr–Mo alloys at 65°C and ambient temperature, there was greater thickness of the oxide film at higher temperature [21]. The high values of E_{tp} showed that formation of the passive film was facilitated under reverse cyclic polarization scanning due to the increase of the cathodic reaction rate. Therefore, an increase in temperature results in competitive and opposite effects since the anodic and cathodic reactions are simultaneously affected by temperature [11,34].

3.2.4. Influence of high anodic polarization

High anodic potential polarization promotes the evolution of oxygen, making the solution more oxidized. According to a previous study [35], the passivity is not disturbed, except under conditions where the oxygen bubbling mechanically damages the passive film. Furthermore, the process only occurs if the oxide film is an electron conductor. Other work has shown that the passive film of S32750 presents a p-n heterojunction [30]. The oxide initially exhibited p-type semiconductor behavior, with cation vacancies being the predominant acceptor species. At high potential,

the material showed n-type semiconductor behavior, with the predominant donor species being oxygen vacancies and/or cation interstitials.

According to the mechanism of film dissolution and growth on stainless steels proposed by Betova *et al.* [36], film growth is promoted when the oxides are acceptors of cation vacancies, while dissolution is stimulated when there is donation of oxygen vacancies and/or cation interstitials. Charge transfer occurs if there is an energy gap between the Fermi level of the semiconductor passive layer and the electrolyte redox potential. In the case of n-type semiconductors, the electrons move from the anode to the solution by electron carriers, resulting in a net positive charge. The direction of the electrons is reversed in the case of p-type semiconductors, with transfer from the solution to the anode resulting in a net negative charge. Hence, oxygen evolution at the anode only occurs if the semiconductor is p-type, since electron withdrawal from water is required to promote water oxidation [36].

The Mott–Schottky (M–S) curves for S32760 and S32750 (Fig. 6) were qualitatively similar, with the same electronic character indicative of p-n heterojunction behavior [9–11]. The passive film on SDSSs presents a typical duplex structure, according to the properties of the oxide formed on the surface, and is characterized as either n-type oxide (left side) or p-type oxide (right side) [37–42]. The n-type peak is attributed to Fe oxides and the p-type to Cr oxides owing to the region of thermodynamic stability of these oxides under the conditions of pH and potential employed in accordance with the Pourbaix diagram [32]. Paredes *et al.* [43] confirmed the appearance of only n-type oxides during M–S tests with carbon steels, in agreement with other studies in which the n-type peak was attributed to Fe oxides [37–42]. Therefore, according to literature, the left peak (p-type) is associated with Fe oxides, while the right peak (n-type) is due to Cr oxides. Hence, the passive films exhibited a duplex character. The p-type character of the passive film could be attributed to the Cr oxides, while the n-type behavior was due to the Fe oxides. A clear difference between the stainless steels was observed in Fig. 6. The peak of the M–S curve attributed to the Cr oxide of S32760 was smaller than the S32750 peak. Therefore, the capacitive effect of the Cr oxide of S32760 was smaller. In the case of the Fe oxide, the S32760 steel presented a large peak. The presence of a Cr-rich deleterious phase in S32760, resulting from interaction with NaOH, could explain the M–S curve results as the presence of the deleterious phase maintained the exposure of Fe in the matrix, while the Cr was less exposed.

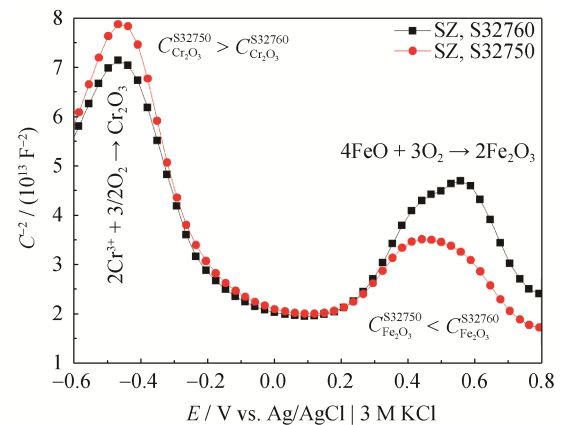


Fig. 6. Mott–Schottky plots for the stir zones of UNS S32760 and S32750 passivated under open circuit potential conditions in 0.5 M Na₂SO₃ + 0.1 M NaCl.

The M–S test (Fig. 6) was performed at pH 9.6 with an applied maximum potential of 0.8 V vs. Ag/AgCl (or 2.74 V vs. RHE, according to Eq. (1)) [44–46]. M–S plots at this potential showed that S32750 and S32760 presented n-type behavior. Despite the use of a high potential, oxygen evolution at the anode did not occur and the passivation process was not affected [36]. This was corroborated by the polarization curves (Fig. 4), which did not show an increase in the current density with increasing applied potential, which would be characteristic of oxygen evolution at the anode [25].

Under the conditions used, the materials remained in a transpassive state for a longer time and dissolution was promoted. This enabled greater distinction of the repassivation processes by microscopy analyses, with the SDSS without a deleterious phase (S32750) presenting better performance. The absence of a deleterious phase facilitates oxide formation during the reverse polarization, with the chromium leaving the metal matrix and becoming oxidized to Cr³⁺. Reaction with oxygen forms Cr₂O₃ according to the mechanism proposed by Betova *et al.* [36]. In the presence of a deleterious phase, chromium does not react to form the passive film. The influence of high anodic polarization in the cyclic analyses on the surface characteristics of the steel was investigated using SEM.

3.3. Surface characteristics of SDSS after the cyclic polarization measurements

After the electrochemical tests, the samples were analyzed by SEM. The SDSS UNS S32760 presented a much larger corroded region than S32750 (Figs. 7 and 8), confirming worse corrosion resistance. The breakdown of the passive film and subsequent metal dissolution were associated with high anodic potential polarization, so it was not representative of a real corrosion situation.

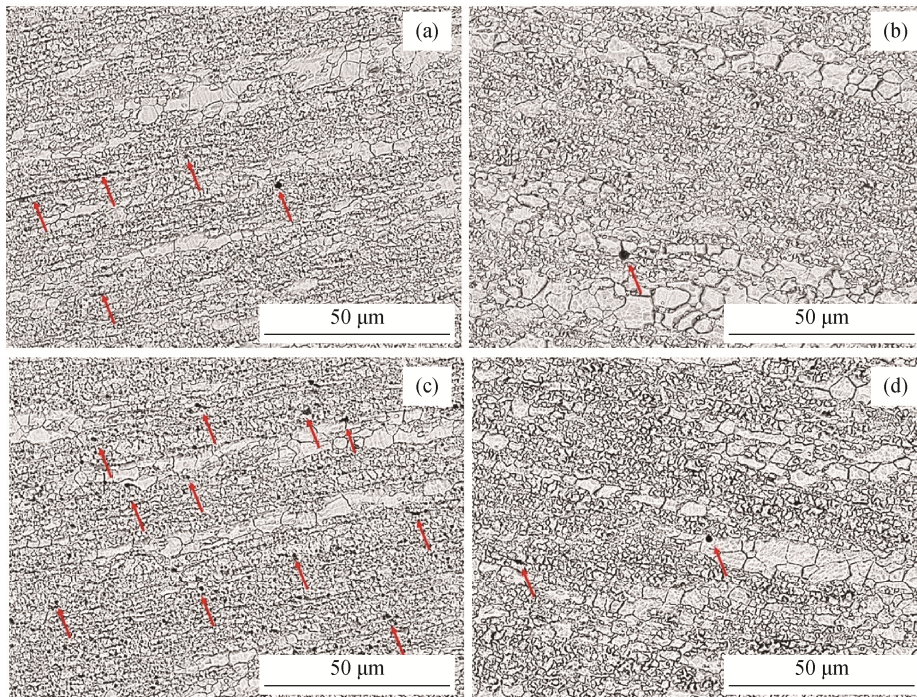


Fig. 7. SEM images of SDSS S32750 after the cyclic polarization tests at pH 5.9 and temperatures of 25°C (a) and 65°C (b), and at pH 3.0 and temperatures of 25°C (c) and 65°C (d). Electrochemical etching: 60vol% HNO₃ in distilled water.

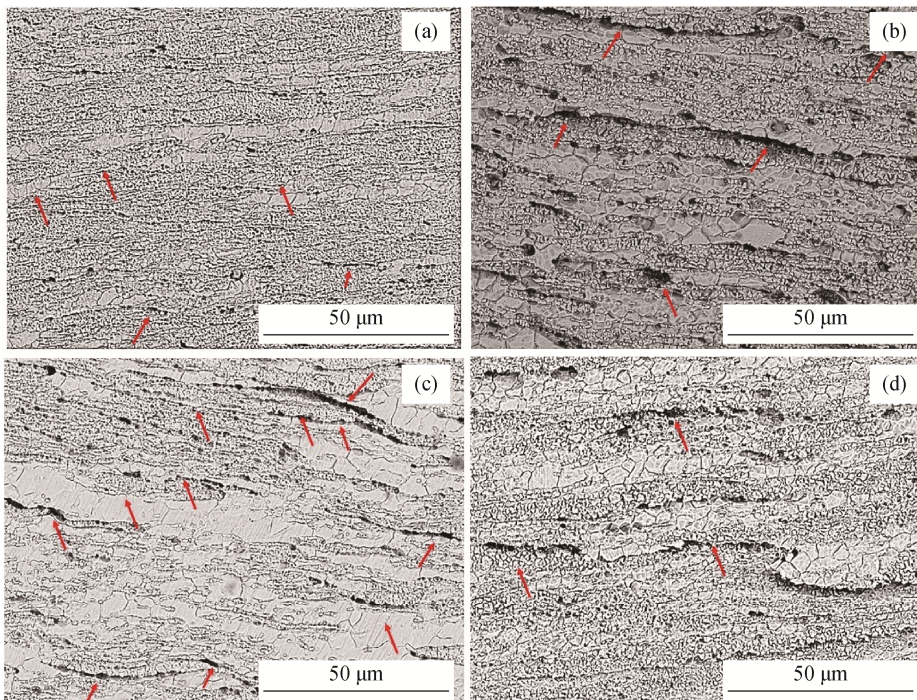


Fig. 8. SEM images of SDSS S32760 after cyclic polarization tests at pH 5.9 and temperatures of 25°C (a) and 65°C (b), and at pH 3.0 and temperatures of 25°C (c) and 65°C (d). Electrochemical etching: 60vol% HNO₃ in distilled water.

In addition to comparison of the relative corrosion resistances of S32750 and S32760, the high anodic polarization enabled analysis of the effects of temperature and pH value on the repassivation process. The SEM images (Figs. 7 and

8) showed that the points of corrosion (indicated by arrows) decreased in acid pH and under high temperature, reflecting superior passive behavior of the SDSSs under these environment conditions. Therefore, a high temperature facili-

tated the repassivation process due to the enhancement of the passivation kinetics [30].

The effect of temperature was also evident at pH 5.9 in the case of the S32750 FSW joint. However, under the same conditions, it was not evident for the S32760 FSW joint likely due to the presence of a deleterious phase. As previously discussed, Fig. 3 shows some of the affected areas at the ferrite–ferrite boundaries, after exposure to NaOH solution, which could be due to the presence of a deleterious intermetallic phase according to ASTM A923. Detrimental chi phase ($\text{Fe}_{18}\text{Cr}_6\text{Mo}_5$) [47] precipitates in SDSS exposed to high temperatures [22–23], especially at ferrite–ferrite interfaces [25,48]. As previously reported [49–51], the effect of W retards the sigma phase kinetics by shifting the sigma phase stability field to the right, allowing the formation of the chi phase during a slightly longer period. Furthermore, the chi phase precedes the sigma phase [49]. These results suggested that although the FSW process only exposed the material to a high temperature for a short time [22], it was sufficient to form the chi phase. There were indications of affected areas at the ferrite–ferrite grain boundaries, with higher exposure of iron oxide and lower exposure of chromium oxide, according to the M–S curves. This could be associated with less chromium available to protect the material, due, for example, to the presence of a phase richer in chromium. In addition, the SEM images of the S32760 FSW joints showed much larger corroded areas. This evidence, together with the lower capacity to promote repassivation after cyclic polarization and the smaller capacitance peak attributed to Cr oxide, was strongly indicative of the presence of a detrimental phase, in agreement with the reduced corrosion resistance.

4. Conclusions

Electrochemical analyses of the UNS S32750 and S32760 SDSSs submitted to FSW were performed by cyclic polarization in 3.5wt% NaCl. The results revealed repassivation behavior under high anodic polarization under different conditions of pH values and temperatures. The following conclusions were obtained.

(1) S32760 showed affected areas at the boundaries of the ferrite–ferrite grains after NaOH etching, which was indicative of the possible presence of a deleterious intermetallic phase after the welding process.

(2) The cyclic polarization curves showed better resistance of S32750 compared to S32760. At pH 3.0, both S32750 and S32760 showed improved passive behavior due to the presence of Mo in the chemical composition of these

SDSSs. Despite the increase in passive behavior, at pH 3.0 the corrosion current density was substantially higher than at pH 5.9. This was probably due to the addition of HCl to obtain an acidic medium, with the high amounts of Cl^- in the pH 3.0 solution acting enhancing the dissolution of S32750 and S32760.

(3) A higher temperature induced competitive effects because the anodic and cathodic reactions were increased. Passivation occurs as a result of cathodic reactions, so the increase of such reactions led to an increase in the passivation kinetics. This effect was evidenced by the SEM images acquired after the polarization tests as fewer corrosion points were observed for the test performed at 65°C. When the high temperature effect was combined with pH 3.0, a decrease in the number of corrosion points was also observed owing to the better passive behavior.

(4) The high anodic polarization did not influence formation of the passive oxide as the oxide exhibited n-type conductor behavior, indicating that oxygen evolution at the anode did not occur. Therefore, the repassivation process can be analyzed by the application of high anodic polarization.

Acknowledgements

The authors thank FACEPE, CNPq, and UFPE for financial support, and CETENE for electrochemical measurements. The SDSS steel plates were kindly donated by Outokumpu (S32750) and Weir Materials (S32760). Scholarships were provided by CNPq.

References

- [1] M.F. McGuire, *Stainless Steels for Design Engineers*, ASM International, Ohio, 2008.
- [2] S.S.M. Tavares, J.M. Pardal, L.D. Lima, I.N. Bastos, A.M. Nascimento, and J.A. de Souza. Characterization of microstructure, chemical composition, corrosion resistance and toughness of a multipass weld joint of superduplex stainless steel UNS S32750, *Mater. Charact.*, 58(2007), No. 7, p. 610.
- [3] R.S. Mishra and M.W. Ma, Friction stir welding and processing, *Mater. Sci. Eng. R*, 50(2005), No. 1-2, p. 1.
- [4] M.K. Mishra, G. Gunasekaran, A.G. Rao, B.P. Kashyap, and N. Prabhu, Effect of multipass friction stir processing on mechanical and corrosion behavior of 2507 super duplex stainless steel, *J. Mater. Eng. Perform.*, 26(2017), No. 2, p. 849.
- [5] M. Atapour, H. Sarlak, and M. Esmailzadeh, Pitting corrosion susceptibility of friction stir welded lean duplex stainless steel joints, *Int. J. Adv. Manuf. Technol.*, 83(2016), No. 5-8, p. 721.
- [6] Z.Q. Zhang, H.Y. Jing, L.Y. Xu, Y.D. Han, L. Zhao, and J.L. Zhang, Influence of microstructure and elemental partitioning

- on pitting corrosion resistance of duplex stainless steel welding joints, *Appl. Surf. Sci.*, 394(2017), p. 297.
- [7] T. Takei, M. Yabe, and F.G. Wei, Effect of cooling condition on the intergranular corrosion resistance of UNS S32506 duplex stainless steel, *Corros. Sci.*, 122(2017), p. 80.
- [8] F. Iacoviello, V. Di Cocco, and L.D. Agostino, Intergranular corrosion susceptibility analysis in stainless steels (duplex) stainless steels, *Procedia Struct. Integrity*, 3(2017), p. 276.
- [9] E.E. Oguzie, J.B. Li, Y.Q. Liu, D.M. Chen, Y. Li, K. Yang, and F.H. Wang, The effect of Cu addition on the electrochemical corrosion and passivation behavior of stainless steels, *Electrochim. Acta*, 55(2010), No. 17, p. 5028.
- [10] M. Metikoš-Hukovic, R. Babic, Z. Grubač, Ž. Petrovic, and N. Lajči, High corrosion resistance of austenitic stainless steel alloyed with nitrogen in an acid solution, *Corros. Sci.*, 53(2011), No. 6, p. 2176.
- [11] Z.Y. Cui, L.W. Wang, H.T. Ni, W.K. Hao, C. Man, S.S. Chen, X. Wang, Z.Y. Liu, and X.G. Li, Influence of temperature on the electrochemical and passivation behavior of 2507 super duplex stainless steel in simulated desulfurized flue gas condensates, *Corros. Sci.*, 118(2017), p. 31.
- [12] T.S. Li, L. Liu, B. Zhang, Y. Li, and F.H. Wang, Growth kinetics of metastable pits on sputtered nanocrystalline stainless steel, *Corros. Sci.*, 124(2017), p. 46.
- [13] G.T. Burstein, M. Carboneras, and B.T. Daymond, The temperature dependence of passivity breakdown on a titanium alloy determined by cyclic noise thermometry, *Electrochim. Acta*, 55 (2010), No. 27, p. 7860.
- [14] M.V. Cardoso, S.T. Amaral, and E.M.A. Martini, Temperature effect in the corrosion resistance of Ni-Fe-Cr alloy in chloride medium, *Corros. Sci.*, 50(2008), No. 9, p. 2429.
- [15] P.D. Krell, S.X. Li, and H.B. Cong, Synergistic effect of temperature and HCl concentration on the degradation of Al-SI 410 stainless steel, *Corros. Sci.*, 122(2017), p. 41.
- [16] H.P. Leckie, Effect of pH on the stable passivity of stainless steels, *Corrosion*, 24(1968), No. 3, p. 70.
- [17] K. Sugimoto and Y. Sawada, The role of molybdenum additions to austenitic stainless steels in the inhibition of pitting in acid chloride solutions, *Corros. Sci.*, 17(1977), No. 5, p. 425.
- [18] G.T. Burstein and B.T. Daymond, The remarkable passivity of austenitic stainless steel in sulphuric acid solution and the effect of repetitive temperature cycling, *Corros. Sci.*, 51(2009), No. 10, p. 2249.
- [19] C. Escrivà-Cerdán, E. Blasco-Tamarit, D.M. García-García, J. García-Antón, R. Akid, and J. Walton, Effect of temperature on passive film formation of UNS N08031 Cr-Ni alloy in phosphoric acid contaminated with different aggressive anions, *Electrochim. Acta*, 111(2013), p. 552.
- [20] S.R. Morrison, *Electrochemistry at Semiconductor and Oxidized Metal Electrodes*, Plenum Press, New York, 1980.
- [21] S. Mischler, A. Vogel, H.J. Mathieu, and D. Landolt, The chemical composition of the passive film on Fe₂₄Cr and Fe₂₄Cr₁₁Mo studied by AES, XPS and SIMS, *Corros. Sci.*, 32(1991), No. 9, p. 925.
- [22] T.F.A. Santos, H.S. Idagawa, and A.J. Ramirez, Thermal history in UNS S32205 duplex stainless steel friction stir welds, *Sci. Technol. Weld. Joining*, 19(2014), No. 2, p. 150.
- [23] H.S. Idagawa, T.F.A. Santos, and A.J. Ramirez, Differential evolution algorithm applied to FSW model calibration, *J. Phys. Conf. Ser.*, 490(2014), No. 1, art. No. 012215.
- [24] T.F.A. Santos, E.A. Torres, T.F.C. Hermengildo, and A.J. Ramirez, Development of ceramic backing for friction stir welding and processing, *Weld. Int.*, 30(2016), No. 5, p. 338.
- [25] T.F.A. Santos, E.A. Torres, J.C. Lippold, and A.J. Ramirez, Detailed microstructural characterization and restoration mechanisms of duplex and superduplex stainless steel friction-stir-welded joints, *J. Mater. Eng. Perform.*, 25(2016), No. 12, p. 5173.
- [26] T.F.A. Santos, E.A. Torres, E.B. Fonseca, and A.J. Ramirez, Friction stir welding of duplex and superduplex stainless steels and some aspects of microstructural characterization and mechanical performance, *Mater. Res.*, 19(2016), No. 1, p. 117.
- [27] ASTM International, ASTM A923-14: *Standard Test Methods for Detecting Detrimental Intermetallic Phase in Duplex Austenitic/Ferritic Stainless Steels*, West Conshohocken, PA, 2014.
- [28] T.F.A. Santos, R.R. Marinho, M.T.P. Paes, and A.J. Ramirez, Microstructure evaluation of UNS S32205 duplex stainless steel friction stir welds, *Rem: Rev. Esc. Minas*, 66(2013), No. 2, p. 187.
- [29] E.M. Westin, *Microstructure and Properties of Welds in the Lean Duplex Stainless Steel LDX 2101* [Dissertation], Royal Institute of Technology, Stockholm, 2010.
- [30] W.S. Tait, *An Introduction to Electrochemical Corrosion Testing For Practicing Engineers and Scientists*, Pair O Docs Pubns, Racine, 1994.
- [31] G.T. Burstein, A hundred years of Tafel's Equation: 1905–2005, *Corros. Sci.*, 47(2005), p. 2858.
- [32] N. Takeno, *Atlas of Eh-pH Diagrams: Intercomparison of Thermodynamic Databases*, Geological Survey of Japan Open File Report No. 419, National Institute of Advanced Industrial Science and Technology, Tokyo, 2005.
- [33] P.C. Pistorius and G.T. Burstein, Metastable pitting corrosion of stainless steel and the transition to stability, *Philos. Trans. R. Soc. A*, 341(1992), p. 531.
- [34] C.O.A. Olsson and D. Landolt, Passive films on stainless steels—chemistry, structure and growth, *Electrochim. Acta*, 48(2003), No. 9, p. 1093.
- [35] G.T. Burstein and D. Sazou, *Passivity and Localized Corrosion*, Elsevier Inc., 2016. doi: 10.1016/B978-0-12-803581-8.01589-7.
- [36] I. Betova, M. Bojinov, T. Laitinen, K. Mäkelä, P. Pohjanne, and T. Saario, The transpassive dissolution mechanism of highly alloyed stainless steels I. Experimental results and modelling procedure, 44(2002), No. 2, p. 2675.
- [37] H. Sarlak, M. Atapour, and M. Esmailzadeh, Corrosion behavior of friction stir welded lean duplex stainless steel, *Mater. Des.*, 66(2015), p. 209.
- [38] N.E. Hakiki, B. Maachi, F. Mechehoud, C. Pirri, A. Meh-

- daoui, and J.L. Bubendorff, Structural and semiconductive investigation of passive films and thermally grown oxides on stainless steels, [in] *7th European Stainless Steel Conference*, Como, 2011, p. 58.
- [39] S. Fujimoto and H. Tsuchiya, Semiconductor Property of Passive Films and Corrosion Behavior of Fe–Cr Alloys, [In] Y. Waseda, S. Suzuki, Eds., *Characterization of Corrosion Products on Steel Surfaces*, Springer, Berlin, Heidelberg, 2006, p. 33.
- [40] L.V. Taveira, M.F. Montemor, M. Da Cunha Belo, M.G. Ferreira, and L.F.P. Dick, Influence of incorporated Mo and Nb on the Mott–Schottky behaviour of anodic films formed on AISI 304L, *Corros. Sci.*, 52(2010), No. 9, p. 2813.
- [41] N.B. Hakiki, S. Boudin, B. Rondot, and M. Da Cunha Belo, The electronic structure of passive films formed on stainless steels, *Corros. Sci.*, 37(1995), No. 11, p. 1809.
- [42] S. Ningshen, U.K. Mudali, V.K. Mittal, and H.S. Khatak, Semiconducting and passive films properties of nitrogen-containing type 316LN stainless steel, *Corros. Sci.*, 49(2007), No. 2, p. 481.
- [43] E.C. Paredes, A. Bautista, S.M. Alvarez, and F. Velasco, Influence of the forming process of corrugated stainless steels on their corrosion behaviour in simulated pore solutions, *Corros. Sci.*, 58(2012), p. 52.
- [44] L. Wang, C.Y. Lee, and P. Schmuki, Solar water splitting: preserving the beneficial smaller feature size in porous α -Fe₂O₃ photoelectrodes during annealing, *J. Mater. Chem. A*, 1(2012), No. 2, p. 212.
- [45] D.R. Chowdhury, L. Spiccia, S.S. Amritphale, A. Paul, and A. Singh, A robust iron oxyhydroxide water oxidation catalyst operating under near neutral and alkaline conditions, *J. Mater. Chem. A*, 4(2016), No. 10, p. 3655.
- [46] C.Y. Lin, D. Mersch, D.A. Jefferson, and E. Reisner, Cobalt sulphide microtube array as cathode in photoelectrochemical water splitting with photoanodes, *Chem. Sci.*, 5(2014), No. 12, p. 4906.
- [47] L. Tan and Y. Yang, *In situ* phase transformation of Laves phase from Chi-phase in Mo-containing Fe–Cr–Ni alloys, *Mater. Lett.*, 158(2015), p. 233.
- [48] I.J. Marques, A.A. Vicente, J.A.S. Tenório, and T.F.A. Santos, Double kinetics of intermetallic phase precipitation in UNS S32205 duplex stainless steels submitted to isothermal heat treatment, *Mater. Res.*, 20(2017), Suppl. 2, p. 152.
- [49] S.B. Kim, K.W. Paik, and Y.G. Kim, Effect of Mo substitution by W on high temperature embrittlement characteristics in duplex stainless steels, *Mater. Sci. Eng. A*, 247(1998), No. 1-2, p. 67.
- [50] J.S. Kim and H.S. Kwon, Effects of tungsten on corrosion and kinetics of sigma phase formation of 25% chromium duplex stainless steels, *Corrosion*, 55(1999), No. 5, p. 512.
- [51] A.R. Akisanya, U. Obi, and N.C. Renton, Effect of ageing on phase evolution and mechanical properties of a high tungsten super-duplex stainless steel, *Mater. Sci. Eng. A*, 535(2012), p. 281.